CHARACTERIZATION OF THE MATRIX AND FUSION CRUST OF THE RECENT METEORITE FALL OZERKI L6

A.A. Maksimova[1], E.V. Petrova[1], A.V. Chukin[1], M.S. Karabanalov[2], I. Felner[3], M. Gritsevich[1,4,5], M.I. Oshtrakh[1,✉]

*[1]Institute of Physics and Technology, Ural Federal University,
Ekaterinburg, 620002 Russian Federation;
[2]Institute of Material Science and Metallurgy, Ural Federal University,
Ekaterinburg, 620002 Russian Federation;
[3]Racah Institute of Physics, The Hebrew University, Jerusalem, 91904 Israel;
[4]Department of Physics, University of Helsinki, Gustaf Hällströmin katu 2a, P.O. Box 64, FI-00014
Helsinki, Finland;
[5]Finnish Geospatial Research Institute, Geodeetinrinne 2, 02430, Masala, Finland*

Abstract

We studied the interior and the fusion crust of the recently recovered Ozerki L6 meteorite using optical microscopy, scanning electron microscopy (SEM) with energy dispersive spectroscopy, X-ray diffraction (XRD), magnetization measurements and Mössbauer spectroscopy. The phase composition of the interior and of the fusion crust were determined by means of SEM, XRD and Mössbauer spectroscopy. The unit cell parameters for silicate crystals were evaluated from the X-ray diffractograms and were found the same for the interior and the fusion crust. Magnetization measurements revealed a decrease of the saturation magnetic moment in the fusion crust due to a decrease of Fe-Ni-Co alloy content. Both XRD and Mössbauer spectroscopy show the presence of magnesioferrite in the fusion crust. The temperatures of cation equilibrium distribution between the M1 and M2 sites in silicates calculated using the data obtained from XRD and Mössbauer spectroscopy appeared to be in a good consistency: 553 K and 479 K for olivine and 1213 K and 1202 K for orthopyroxene.

✉Author for correspondence: E-Mal: oshtrakh@gmail.com

Introduction

On June 21, 2018 at 01:16:20 UT, an exceptionally bright fireball was witnessed in the Lipetsk Region, Russian Federation as well as in neighboring areas. An analysis of the fireball trajectory, following Lyytinen and Gritsevich (2016) and references therein, was clearly indicative of a number of meteorite fragments survived through atmospheric entry and landed on the ground. A meteorite expedition from the Ural Federal University initiated a meteorite recovery campaign that successfully recovered the first meteorite fragments within 2 days from the fall. The meteorite was classified as ordinary chondrite L6 with a shock stage S4/5 and weathering grade W0 and named Ozerki (*Meteoritical Bulletin*, 2018, no 107).

One of the Ozerki L6 meteorite fragments was chosen for the study using optical microscopy, scanning electron microscopy (SEM) with energy dispersive spectroscopy (EDS), X-ray diffraction (XRD), magnetization measurements and Mössbauer spectroscopy with a high velocity resolution. Additionally, the fusion crust from this fragment was also studied by these techniques.

Materials and methods

The studied Ozerki L6 meteorite fragment is shown in Fig. 1. A thin layer of the fusion crust is present at the fragment's surface. This fragment was cut, and polished thin section was prepared using the standard method. The polished thin section was then characterized by optical microscopy and SEM with EDS. Then powdered matter was removed from the polished thin section for further study by means of XRD, magnetization measurements and Mössbauer spectroscopy. For Mössbauer spectroscopy, a powdered material was glued onto Al foil free from Fe with a thickness of ~6 mg Fe/cm^2. Similarly, a powdered fusion crust was prepared for the study by these techniques.

An Axiovert 40 MAT microscope (Carl Zeiss) was used for optical microscopy characterization of Ozerki L6 fragment. Scanning electron-ion microscope Auriga CrossBeam (Carl Zeiss) was used for SEM analysis while EDS device X-max 80 (Oxford Instruments) was applied for the analysis of chemical composition of Ozerki L6. XRD analyses were done on the interior and fusion crust using the XRD–7000 powder diffractometer (Shimadzu) operated at 40 kV and 30 mA with CuK_α radiation using a monochromator, scanned over 2Θ from 12° to 86° with a step of 0.03° per 10 s. The XRD patterns were fitted using PANalytical X'Pert High Score Plus software with the Rietveld full profile analysis and ICDD PDF2 database. Magnetization measurements were carried out using commercial SQUID MPMS-5S magnetometer (Quantum Design) on a few mg of the powdered samples, in the temperature range of 5 to 295 K. The differential SQUID sensitivity was 10^{-7} emu. The sample was cooled to 5 K and the field (90 Oe) was switched on to trace the zero-field-cooled (ZFC) branch of the magnetization M(T) curve. The magnetometer was adjusted to be in a real H=0 state prior to recording the ZFC curve. Under this field, the field-cooled (FC) branch was measured via heating from 5 to 295 K.

An automated precision Mössbauer spectrometric system was used for ^{57}Fe Mössbauer spectra measurement. This system was built on the base of the SM-2201 spectrometer operating with a saw-tooth shape velocity reference signal. This signal is formed by the digital-analog converter using discretization of 2^{12} (the velocity quantification using 4096 steps). The high level of velocity scale discretization provides much better adjusting to resonance and significantly increases the spectra quality and possibilities to reveal small overlapping spectral components with respect to conventional Mössbauer setups with a considerably lower level of the velocity reference signal discretization. Descriptions of this spectrometer and the system were presented elsewhere (Oshtrakh et al., 2009; Semionkin et al., 2010; Oshtrakh and Semionkin, 2013, 2016). The ~1.0×10^9 Bq ^{57}Co(Rh) source (Ritverc GmbH, St. Petersburg, Russian Federation) was used at room temperature. The 295 K Mössbauer spectra were measured in transmission geometry with moving absorber, which excludes parabolic distortion of the spectral base line, and recorded in 4096 channels. For their analysis, the spectra of Ozerki L6 interior and the fusion crust were converted into 1024 channels by a consequent summation of four neighboring channels to increase the signal-to-noise ratio for the minor spectral components. The statistical rates in the spectra were ~9.8×10^6 and ~10.4×10^6 counts per channels and signal-to-noise ratios were 217 and 233 for the powdered internal bulk material and the fusion crust spectra, respectively. Each spectrum was measured for 16 days to reach the signal-to-noise ratio appropriate for reliable fits of the smallest spectral components. Mössbauer spectra were computer fitted with the least squares procedure using UNIVEM-MS program with a Lorentzian line shape. The line shapes of the Mössbauer spectrum of the reference absorber of α-Fe foil (the thickness of ~7 μm) were pure Lorentzian. The line widths (Γ, the full width at a half maximum) in the 1024-channel spectrum of α-Fe foil were $\Gamma_{1,6} = 0.228\pm0.030$ mm/s, $\Gamma_{2,5} = 0.227\pm0.030$ mm/s and $\Gamma_{3,4} = 0.216\pm0.030$ mm/s for the 1st and the 6th, the 2nd and the 5th, the 3rd and the 4th peaks in sextet, respectively. Velocity resolution (velocity per one channel) in the 1024-channel Mössbauer spectra was ~0.015 mm/s per channel for the powdered material and ~0.019 mm/s per channel for the fusion crust due to the different velocity ranges used for these spectra measurements. The spectral parameters such as: isomer shift, δ, quadrupole splitting, ΔE_Q, quadrupole shift for magnetically split components, ε $(2\varepsilon=\Delta E_Q)$, magnetic hyperfine field, H_{eff}, line width, Γ, relative subspectrum (component) area, A, and

normalized statistical quality of the fit, χ^2, were determined. Criteria for the best fit were the differential spectrum (the difference between experimental and calculated spectral points), χ^2 values and physical meaning of parameters. An instrumental (systematic) error for each spectrum point was equivalent to ±0.5 channel (the velocity scale) while that for the hyperfine parameters was equivalent to ±1 channel (in mm/s or kOe). If an error calculated with the fitting procedure (fitting error) for these parameters exceeded the instrumental (systematic) error the larger error was used instead. The instrumental relative error for A was estimated to be ≤10 % (the values of A are given in tables as calculated in the fit with two decimal digits to keep the total relative area equal to 100 %). Values of δ are given relative to α-Fe at 295 K.

Results and discussion

The interior

Selected optical microphotographs of the Ozerki L6 polished thin section obtained in non-polarized and polarized light are shown in Fig. 2. Some phases such as Fe-Ni-Co alloy grains, troilite and chromite inclusions were found in silicate matrix consisting of olivine and pyroxenes. It was interesting to observe a part of troilite inclusions with a high grade of porosity. Selected SEM images of Ozerki L6 polished thin section are shown in Fig. 3 (additional images can be found in Fig. S1 in Supporting Information). These images showed the presence of Fe-Ni-Co grains with different α-, $α_2$- and γ-phases which differ in the Ni content. Some grains contained 30–33 at.% of Ni that corresponds to the presence of the paramagnetic γ-Fe(Ni, Co) phase. Chromite grains were found with Al as the third largest metal content in addition to Cr and Fe. This means that chromite may contain some part of hercynite ($FeAl_2O_4$) or mixed Al and Cr spinel. Troilite inclusions were observed as homogeneous particles and as particles with high level of porosity, probably, a mixture of troilite with silicate matrix. The content of metals in different minor iron-bearing phases is shown in Table 1.

Analysis of the XRD pattern of the bulk material from Ozerki L6 ordinary chondrite (see Fig. S2 in Supporting Information) showed the presence of olivine (50.6 wt.%), orthopyroxene (23.0 wt.%), anorthite (14.4 wt.%), troilite (4.5 wt.%), Ca-rich clinopyroxene (3.3 wt.%), the α-Fe(Ni, Co) phase (1.8 wt.%), chromite (1.5 wt.%), the γ-Fe(Ni, Co) phase (0.4 wt.%), hercynite (0.3 wt.%) and chlorapatite $Ca_5(PO_4)_3Cl$ (0.2 wt.%). The unit cell parameters were evaluated using the Rietveld full profile analysis for olivine, orthopyroxene and Ca-rich clinopyroxene found in Ozerki L6 (Table 2).

The M(T) ZFC and FC and M(H) measurements of the bulk material from Ozerki L6 ordinary chondrite are shown in Fig. 4. Two peaks around 18 and 58 K are observed in the ZFC branch. The higher peak is attributed to the ferrimagnetic chromite (Gattacceca et al., 2011) and the peak at 18 K is probably due to hercynite $FeAl_2O_4$ because its Curie temperature (T_C) is around 15 K (Gattacceca et al., 2011, Klemme and van Miltenburg, 2003, Sack and Ghiorso, 1991). Both transitions are also observed in the FC branch. Note, that the two branches do not merge at 295 K, indicating other magnetic phase(s) which order well above room temperature.

The isothermal magnetization M(H) curves of Ozerki L6 measured at 5 and 295 K up to 45000 Oe are also depicted in Fig. 4. In both cases, M(H) first increases linearly up to 3000–4000 Oe and then tends to saturate. The M(H) plots clearly reveal an admixture of at least two components and can be fitted as: $M(H) = M_S + \chi_p H$, where M_S corresponds to the intrinsic magnetic saturation moment and $\chi_p H$ is the linear paramagnetic part. At 5 and 295 K the M_S values are 51.1 and 46.7 emu/g, respectively, and related to Fe-Ni-Co alloy (see Gattacceca et al., 2014). The slight loss in the saturation moments (8.6%), indicates that this alloy in Ozerki L6 orders at elevated temperatures. That is consistent with the shown M(T) plots.

Mössbauer spectrum of the bulk material of Ozerki L6 ordinary chondrite is shown in Fig. 5. This spectrum is similar to other L ordinary chondrites (see Maksimova and Oshtrakh, 2019 and references therein). To fit this spectrum well, we used an approach to simulate the full static

Hamiltonian to fit troilite component in the complex Mössbauer spectra of ordinary chondrites that was described in detail by Maksimova et al. (2014, 2016, 2017) and Oshtrakh et al. (2016). We also accounted for spectral components related to the ^{57}Fe in the M1 and M2 sites in silicate crystals and different phases for Fe-Ni-Co alloy as well as a component associated with hercynite for the fitting model. The result of the best fit is shown in Fig. 5. The obtained Mössbauer parameters for spectral components are given in Table 3. The assigning of spectral hyperfine parameters to the indicated compounds (phases) was done in the same way as it was recently done in the studies of other ordinary chondrites (see Maksimova et al., 2018b; Oshtrakh et al., 2019; and references therein). It should be noted that we were unable to calculate correctly the spectral components which could be assigned to the M1 and M2 sites in clinopyroxene. This is a result of a very low content of clinopyroxene (XRD showed the presence of ~3 wt.% of clinopyroxene). In case of a low content of clinopyroxene, its low-intensity spectral components overlapping with high-intensity spectral components of orthopyroxene cannot be revealed well without significant increase in correlation of their parameters. The same was found in the case of the Mössbauer spectrum of Chelyabinsk LL5 fragment No 1 with the presence of 3.9 wt.% of clinopyroxene. In the other Chelyabinsk fragments that had larger clinopyroxene content, these components were revealed in the Mössbauer spectra (Oshtrakh et al., 2019).

If we assume the same Mössbauer effect probability (the *f*-factor) for all phases in Ozerki L6 we can roughly estimate the iron fraction in all iron-bearing minerals (by using relative areas of spectral components) and compare with some recently studied ordinary chondrites Northwest Africa 6286 LL6, Chelyabinsk LL5 (fragments No 1 and No 2) and Tsarev L5 (Maksimova et al., 2018a, 2018b; Oshtrakh et al., 2019). For example, the metal content in Ozerki L6 is slightly larger than that for the three LL chondrites. Following the assumption about the same *f*-factor for all phases, we can roughly estimate the Fe^{2+} fractions (occupancies) in the M1 and M2 sites (X_{Fe}^{M1} and X_{Fe}^{M2}) in silicate crystals in Ozerki L6 meteorite. The ratios of X_{Fe}^{M1}/X_{Fe}^{M2} are equal to corresponding ratios of the subspectra relative areas A^{M1}/A^{M2}. On the other hand, the Rietveld full profile analysis can obtain directly the X_{Fe}^{M1} and X_{Fe}^{M2} from the Ozerki L6 XRD pattern. Therefore, it is possible to compare X_{Fe}^{M1}/X_{Fe}^{M2} for olivine and orthopyroxene using two independent techniques (see Table 4). A good consistency of X_{Fe}^{M1}/X_{Fe}^{M2} values obtained using the data from XRD and A^{M1}/A^{M2} values from Mössbauer spectroscopy is clearly seen in Table 4.

The distribution of Fe^{2+} and Mg^{2+} cations between the M1 and M2 sites in orthopyroxene and, probably, in olivine is related to the minerals' thermal history. Using the distribution coefficient $K_D = (X_{Fe}^{M1} \times X_{Mg}^{M2})/(X_{Fe}^{M2} \times X_{Mg}^{M1})$ it is possible to determine the temperature of equilibrium cation distribution T_{eq}. The Fe^{2+} and Mg^{2+} occupancies were determined from XRD (see Table 4, $X_{Fe}^{M1} + X_{Mg}^{M1} = 1$). Therefore, the values of K_D for olivine and orthopyroxene that were calculated from these data are 1.58 and 0.24, respectively. To determine T_{eq}, we used equations for olivine: $-\Delta G = R \times T_{eq} \times \ln K_D$, where the Gibbs energy $\Delta G = 20935$ J for olivine, $R = 8.31$ J/K mol (Malysheva, 1975), and for orthopyroxene: $\ln K_D = 0.391 - 2205/T_{eq}$ (Wang et al., 2005). Calculated values of T_{eq} are 553 K and 1213 K for olivine and orthopyroxene, respectively. Using relative areas of corresponding spectral components in the Mössbauer spectrum of Ozerki L6 we can calculate K_D and T_{eq} for olivine and orthopyroxene also using the values of fayalite (Fa) and ferrosilite (Fs) for this meteorite by means of approach described in detail by Oshtrakh et al. (2008, 2019). The values of Fa and Fs are 0.26 and 0.21 (*Meteoritical Bulletin*, 2018, no 107). The values of K_D and T_{eq} calculated from Mössbauer data are: 1.69 and 479 K for olivine and 0.24 and 1202 K for orthopyroxene. The results obtained using two independent techniques are in a good consistency. Moreover, the values of T_{eq} calculated by two techniques for orthopyroxene in Ozerki L6 agree with the T_{eq} range of 1085–1207 K calculated by Slater-Reynolds and McSween (2005) for orthopyroxene in L6 ordinary chondrites.

The relative areas of components in the Mössbauer spectra of ordinary chondrites can be used for meteorites classification as has already been shown by Paliwal et al. (2000), Verma et al. (2002, 2003), Verma and Tripathy (2004), Oshtrakh et al. (2008), Galazka-Friedman et al. (2017) and Elewa and Cadogan (2017). We used this approach also and found that the plot of the total relative

area of components related to Fe-Ni-Co alloy plus those assigned to Fe^{3+} compounds versus the total relative area of components associated with the M1 and M2 sites in olivine can be considered as the most useful for classification (Oshtrakh et al., 2008, 2019; Maksimova et al., 2017, 2018b; Maksimova and Oshtrakh, 2019). This way is possible for non-weathered meteorites and in situations with small weathering grade when iron in silicate crystals is not oxidized. In the plot shown in Fig. 6 for ordinary chondrites from H, L and LL groups studied in the above mentioned our papers, Ozerki L6 falls in the L ordinary chondrites region.

The fusion crust

The fusion crust can be seen in Fig. 1 at the surface of Ozerki L6 fragment. Microphotographs of this fusion crust obtained in non-polarized and polarized light are shown in Fig. 7 (microphotographs of the glass-like surface with higher magnification are shown in Fig. S3 in Supporting Information). These microphotographs showed the glass-like crust surface and the second and the third crust layers (see Rubin, 1997) with inclusions of the Fe-Ni-Co grains and chromite particles. SEM images of the Ozerki L6 fusion crust (Fig. 8) also demonstrate the glass-like surface, the second (intermediate) and the third (inner) crust layers with inclusions of the troilite-Fe-Ni-Co grain associations and chromite. The third layer contains many troilite – Fe-Ni-Co veins (Fig. 8 and Fig. S4 in Supporting Information) resulting from rapidly solidified FeS and Fe-Ni-Co alloy intergrowth (Rubin, 1997). The glass-like surface shows the formation of fractal-like dendritic crystals (Fig. S5 in Supporting Information) which indicate rapid solidification of the molten matter in the crust. EDS analysis showed that: (i) dendritic crystals consist of silicates like pyroxene with a higher Fe content (~5–10 at.%) and a smaller Mg content (~10–6 at.%), (ii) chromite contains ~3 at.% of Al as the third metal after Cr and Fe that indicates the possible presence of hercynite in chromite crystals, (iii) troilite consists of ~55–52 at.% of S and ~45–48 at.% of Fe, (iv) metal grains consist of the α-Fe(Ni, Co) phase with Ni and Co contents of ~3 at.% and ~2 at.%, respectively, and the α_2-Fe(Ni, Co) phase with Ni and Co contents of ~14 at.% and ~2–2.5 at.%, respectively.

XRD pattern of the Ozerki L6 fusion crust is shown in Fig. 9. This pattern was fitted using the Rietveld full profile analysis which determined the following composition of the crust: olivine (58.8 wt.%), orthopyroxene (14.8 wt.%), magnesioferrite $MgFe_2O_4$ (13.1 wt.%), anorthite (7.6 wt.%), troilite (2.0 wt.%), Ca-rich clinopyroxene (1.6 wt.%), the α-Fe(Ni, Co) phase (1.0 wt.%), chromite (0.5 wt.%), hercynite (0.4 wt.%) and the γ-Fe(Ni, Co) phase (0.2 wt.%). The unit cell parameters for silicate crystals in the fusion crust were the same as those for silicate crystals in the bulk material shown in Table 2. A large amount of magnesioferrite was observed in the fusion crust of Ozerki L6 similar to that found by XRD in the fusion crust from Saratov L4 and two fragments of Chelyabinsk LL5 ordinary chondrites (Yudin et al., 1968; Maksimova et al., 2014; Oshtrakh et al., 2019). In contrast, the majority of previous studies observed magnetite Fe_3O_4 and wüstite FeO in the fusion crust (Rubin, 1997). However, according to PDF 01-089-6188, two main magnesioferrite peaks [2 2 0] and [3 1 1] are clearly seen in Fig. 11 at 2Θ ~30° and ~35.5°, respectively.

The results of magnetization measurements of the fusion crust (Fig. 10) seem to be very similar to that of Ozerki L6's interior shown in Fig. 5. Generally speaking, fusion crust material also contains a mixture of a few magnetic and paramagnetic phases, but with different relative fractions, namely that paramagnetic phase(s) are more dominant. That is readily expressed in (i) the up-rise of the ZFC curve below 12 K and (ii) in the lower M_S values, 26 and 22 emu/g at 5 and 295 K, respectively. That indicates that the magnetic Fe-Ni-Co alloy fraction (with T_C is well above room temperature) is about 50% lower than those obtained for the internal material (Fig. 4), a consequence which confirms the XRD data. We may attribute the broad peaks around 21 and 48–50 K observed in the ZFC branch (Fig. 10, inset) to the same magnetic hercynite and chromite phases as considered above for the interior.

The Mössbauer spectrum of the fusion crust from Ozerki L6 meteorite is shown in Fig. 11. This spectrum demonstrates similar shape as that of the spectra of the fusion crust from

Chelyabinsk LL5 fragments (Oshtrakh et al., 2019). This spectrum was fitted well using 7 magnetic sextets, 6 quadrupole doublets and 1 paramagnetic singlet. Parameters of these components are shown in Table 5. Based on the hyperfine parameters, these components were related to corresponding compounds (phases). Two magnetic sextets with H_{eff} of ~337 and ~312 kOe are related to the α-Fe(Ni, Co) phase and troilite, respectively. Other 5 magnetic sextets were associated with magnesioferrite which has a spinel structure with Fe^{3+} and Mg^{2+} cations in both tetrahedral (A) and octahedral [B] sites within the formula: $(Mg_{1-x}Fe_x)_A[Mg_yFe_{2-y}]_BO_4$. There are 8 metal ions in the (A) sites and 16 metal ions in the [B] sites. Therefore, there is a distribution of different numbers of Fe^{3+} and Mg^{2+} cations in the neighboring coordination spheres of ^{57}Fe in both (A) and [B] sites. This leads to different hyperfine fields on the ^{57}Fe nuclei resulting from these distributions. Two magnetic sextets with δ values of about 0.27 mm/s were assigned to the (A) sites while three magnetic sextets with larger δ values were related to the [B] sites. For example, earlier, De Grave et al. (1979) showed that the Mössbauer spectrum of magnesioferrite can be fitted using 1 magnetic sextet for the (A) sites and 3 magnetic sextets for the [B] sites.

Two pairs of quadrupole doublets were assigned to the M1 and M2 sites in olivine and orthopyroxene, respectively, similar to that in the spectrum of bulk material. Two residual quadrupole doublets demonstrate hyperfine parameters corresponding to ferrous and ferric compounds, however, these compounds were not identified yet. These compounds may be a result of structural modification of silicate crystals with partial oxidation during combustion at the atmosphere. Singlet component has parameters corresponding to chromite. The relative part of Fe-Ni-Co alloy in the fusion crust was found by Mössbauer spectroscopy half than that in the interior. This is in agreement with XRD data and difference for the saturation magnetic moment for the fusion crust and interior of Ozerki L6 meteorite.

Following the above mentioned comparison of the M1 and M2 sites occupancies by Fe^{2+} and their ratios for olivine and orthopyroxene calculated from XRD and Mössbauer spectra data, we carried out this comparison for silicate crystals in the fusion crust of Ozerki L6 meteorite. These results are given in Table 6. The ratios X_{Fe}^{M1}/X_{Fe}^{M2} and A^{M1}/A^{M2} are in a good consistency for olivine and orthopyroxene, respectively, but these values are slightly lower than those calculated for the bulk material (see Table 4). It is well known that annealing of silicate crystals followed by quenching leads to redistribution of Fe^{2+} and Mg^{2+} cations between the M1 and M2 sites (see, for example, Zema et al., 1999; Heinemann et al., 1999; Morozov et al., 2005). Therefore, we can calculate a temperature T_{FC} similarly to T_{eq} for olivine and orthopyroxene underwent high temperature effect during the fusion crust formation using approach applied above for silicates in the interior. The calculated T_{FCeq} values are as follows: 1113 K (XRD) and 927 K (Mössbauer spectroscopy) for olivine and 978 K (XRD) and 962 K (Mössbauer spectroscopy) for orthopyroxene. These values are very close and if calculated temperature can be considered as a temperature of silicate crystals annealing during the final layer of the fusion crust formation, both olivine and orthopyroxene were undergone by heating around 1000 K with fast cooling.

Conclusions

We have studied the sample of the Ozerki L6 meteorite by means of optical microscopy, scanning electron microscopy with energy dispersive spectroscopy, X-ray diffraction, magnetization measurements and Mössbauer spectroscopy. The main iron-bearing phases such as olivine, orthopyroxene, troilite, Ca-rich clinopyroxene, α-Fe(Ni, Co) and γ-Fe(Ni, Co) phases, chromite and hercynite were observed using EDS and XRD in the bulk material. Magnetization measurements demonstrated the magnetic phase transitions of chromite and probably hercynite at 58 and 18 K, respectively. The saturation magnetic moment at 5 K is ~51 emu/g and related to the Fe-Ni-Co alloy mainly, which orders magnetically well-above room temperature. Components assigned to the M1 and M2 sites in olivine and orthopyroxene, troilite, the ferromagnetic α-Fe(Ni, Co) and paramagnetic γ-Fe(Ni, Co) phases, chromite and hercynite were revealed from the Mössbauer spectrum of Ozerki L6. Determination of the Fe^{2+} occupancies of the M1 and M2 sites

in both olivine and orthopyroxene by two independent techniques, XRD and Mössbauer spectroscopy, showed a good agreement. The temperatures of cation equilibrium distribution in silicate phases, calculated basing on the data from these two techniques, were 553 K (XRD) and 479 K (Mössbauer spectroscopy) for olivine and 1213 K (XRD) and 1202 K (Mössbauer spectroscopy) for orthopyroxene. Systematics of ordinary chondrites using the relative areas of Mössbauer spectral components demonstrated that Ozerki L6 corresponds to the L ordinary chondrites region.

The study of the Ozerki L6 fusion crust by the same techniques demonstrated the following. The fusion crust consists of three layers of glass-like, molten and partially molten silicate phases with grains of chromite, Fe-Ni-Co alloy and veins of FeS – Fe-Ni-Co alloy intergrows resulting from rapidly solidified melt. XRD did not reveal any differences in the unit cell parameters for silicate crystals in the fusion crust in comparison with the bulk material. However, XRD revealed chromite and hercynite, a twofold decrease of Fe-Ni-Co alloy and appearance of magnesioferrite as a result of metallic alloy and silicates combustion. Magnetization measurements showed the magnetic phase transitions for chromite around 48 K and at ~21 K probably for hercynite while the saturation magnetic moment at 5 K was found 26 emu/g which is twice smaller than that in the bulk material. The Mössbauer spectrum confirmed a decrease of Fe-Ni-Co alloy content and appearance of magnesioferrite in addition to components related to the M1 and M2 sites in silicate crystals, troilite, chromite and yet unknown ferrous and ferric compounds. Based on the XRD and Mössbauer data the temperature of the fusion crust final layer formation at the Ozerki L6 surface was estimated about 1000 K.

Acknowledgement

References

Dodd R.T. Meteorites: A Petrological-Chemical Synthesis. Cambridge University Press, Cambridge, 1981, 368 pp.

Elewa N.N., Cadogan J.M. 2017. An [57]Fe Mössbauer study of the ordinary chondrite meteorite Lynch 001. *Hyperfine Interact.*, **238**, 4.

Galazka-Friedman J., Wozniak M., Duda P., Rzepecka P., Jakubowska M., Karwowski Ł. 2017. Mössbauer spectroscopy – a useful method for classification of meteorites? *Hyperfine Interact.*, **238**, 67.

Gattacceca J., Rochette P., Lagroix F., Mathé P.-E., Zanda B. 2011. Low temperature magnetic transition of chromite in ordinary chondrites. *Geophys. Res. Lett.*, **38**, L10203.

Gattacceca J., Suavet C., Rochette P., Weiss B.P., Winklhofer M., Uehara M., Friedrich J.M. 2014. Metal phases in ordinary chondrites: Magnetic hysteresis properties and implications for thermal history. *Meteorit. & Planet. Sci.*, **49**, 652–676.

De Grave E., Govaert A., Chambaere D., Robbrecht G. 1979. A Mössbauer effect study of $MgFe_2O_4$. *Physica B*, **96**, 103–110.

Heinemann R., Staack V., Fischer A., Kroll H., Vad T., Kirfel A. 1999. Temperature dependence of Fe,Mg partitioning in Acapulco olivine. *Am. Mineral.*, **84**, 1400–1405.

Jarosewich E. 1990. Chemical analyses of meteorites: A compilation of stony and iron meteorite analyses. *Meteoritics,* **25**, 323–337.

Klemme S., van Miltenburg J.C. 2003. Thermodynamic properties of hercynite ($FeAl_2O_4$) based on

adiabatic calorimetry at low temperatures. *Am. Mineral.*, **88**, 68–72.

Lyytinen E., Gritsevich M. 2016. Implications of the atmospheric density profile in the processing of fireball observations. *Planet. Space Sci.*, **120**, 35–42.

Maksimova A.A., Klencsár Z., Oshtrakh M.I., Petrova E.V., Grokhovsky V.I., Kuzmann E., Homonnay Z., Semionkin V.A. 2016. Mössbauer parameters of ordinary chondrites influenced by the fit accuracy of the troilite component: An example of Chelyabinsk LL5 meteorite. *Hyperfine Interact.*, **237**, 33.

Maksimova A.A., Oshtrakh M.I., Klencsár Z., Petrova E.V., Grokhovsky V.I., Kuzmann E., Homonnay Z., Semionkin V.A. 2014. A comparative study of troilite in bulk ordinary chondrites Farmington L5, Tsarev L5 and Chelyabinsk LL5 using Mössbauer spectroscopy with a high velocity resolution. *J. Mol. Struct.*, **1073**, 196–201.

Maksimova A.A., Oshtrakh M.I., Petrova E.V., Grokhovsky V.I., Semionkin V.A. 2014. Study of Chelyabinsk LL5 meteorite fragment with light lithology and its fusion crust using Mössbauer spectroscopy with a high velocity resolution. In: *Proceedings of the International Conference "Mössbauer Spectroscopy in Materials Science 2014"*, Eds. J. Tuček, M. Miglierini, AIP Conference Proceedings, Melville, New York, **1622**, 24–29.

Maksimova A.A., Oshtrakh M.I., Petrova E.V., Grokhovsky V.I., Semionkin V.A. 2017. Comparison of iron-bearing minerals in ordinary chondrites from H, L and LL groups using Mössbauer spectroscopy with a high velocity resolution. *Spectrochim. Acta, Part A: Molec. and Biomolec. Spectroscopy*, **172**, 65–76.

Maksimova A.A., Kamalov R.V., Chukin A.V., Felner I., Oshtrakh M.I. 2018a. An analysis of orthopyroxene from Tsarev L5 meteorite using X-ray diffraction, magnetization measurement and Mössbauer spectroscopy. *J. Mol. Struct.*, **1174**, 6–11.

Maksimova A.A., Oshtrakh M.I., Chukin A.V., Felner I., Yakovlev G.A., Semionkin V.A. 2018b. Characterization of Northwest Africa 6286 and 7857 ordinary chondrites using X-ray diffraction, magnetization measurements and Mössbauer spectroscopy. *Spectrochim. Acta, Part A: Molec. and Biomolec. Spectroscopy*, **192**, 275–284.

Maksimova A.A., Oshtrakh M.I. 2019. Ordinary chondrites: what can we learn using Mössbauer spectroscopy? *J. Mol. Struct.*, **1186**, 104–117.

Malysheva T.V. 1975. Mössbauer effect in geochemistry and cosmochemistry. Moscow, Nauka, pp. 166 (in Russian).

Morozov M., Brinkmann C., Lottermoser W., Tippelt G., Amthauer G., Kroll H. 2005. Octahedral cation partitioning in Mg,Fe^{2+}-olivine. Mössbauer spectroscopic study of synthetic $(Mg_{0.5}Fe^{2+}_{0.5})_2SiO_4$ (Fa_{50}). *Eur. J. Mineral.*, **17**, 495–500.

Oshtrakh M.I., Maksimova A.A., Klencsár Z., Petrova E.V., Grokhovsky V.I., Kuzmann E., Homonnay Z., Semionkin V.A. 2016. Study of Chelyabinsk LL5 meteorite fragments with different lithology using Mössbauer spectroscopy with a high velocity resolution. *J. Radioanal. Nucl. Chem.*, **308**, 1103–1111.

Oshtrakh M.I., Maksimova A.A., Chukin A.V., Petrova E.V., Jenniskens P., Kuzmann E., Grokhovsky V.I., Homonnay Z., Semionkin V.A. 2019. Variability of Chelyabinsk meteoroid stones studied by Mössbauer spectroscopy and X-ray diffraction. *Spectrochim. Acta, Part A: Molec. and Biomolec. Spectroscopy*, **219**, 206–224.

Oshtrakh M.I., Petrova E.V., Grokhovsky V.I., Semionkin V.A. 2008. A Study of Ordinary Chondrites by Mössbauer Spectroscopy with High-Velocity Resolution. *Meteoritics & Planetary Sci.*, **43**, 941–958.

Oshtrakh M.I., Semionkin V.A. 2013. Mössbauer spectroscopy with a high velocity resolution: advances in biomedical, pharmaceutical, cosmochemical and nanotechnological research. *Spectrochim. Acta, Part A: Molec. and Biomolec. Spectroscopy*, **100**, 78–87.

Oshtrakh M.I., Semionkin V.A. 2016. Mössbauer Spectroscopy with a High Velocity Resolution: Principles and Applications, in Proceedings of the International Conference "Mössbauer Spectroscopy in Materials Science 2016" (Tuček J., Miglierini M., eds.), AIP Conference Proceedings. AIP Publishing, Melville, New York, **1781**, 020019.

Oshtrakh M.I., Semionkin V.A, Milder O.B., Novikov E.G. 2009. Mössbauer spectroscopy with high velocity resolution: an increase of analytical possibilities in biomedical research. *J. Radioanal. Nucl. Chem*., **281**, 63–67.

Paliwal B.S., Tripathi R.P., Verma H.C., Sharma S.K. 2000. Classification of the Didwana-Rajod meteorite: a Mössbauer spectroscopic study. *Meteorit. & Planet. Sci*., **35**, 639–642.

Rubin A.E. Mineralogy of meteorite groups. 1997. *Meteorit. & Planet. Sci*., **32**, 231–247.

Sack R.O., Ghiorso M.S. 1991. An internally consistent model for the thermodynamic properties of Fe- Mg-titanomagnetite-aluminate spinels. *Contrib. Mineral. Petrol*., **106**, 474–505.

Semionkin V.A., Oshtrakh M.I., Milder O.B., Novikov E.G. 2010. A high velocity resolution Mössbauer spectrometric system for biomedical research. *Bull. Rus. Acad. Sci.: Phys*., **74**, 416–420.

Slater-Reynolds V., McSween H.Y., Jr. 2005. Peak metamorphic temperatures in type 6 ordinary chondrites: An evaluation of pyroxene and plagioclase geothermometry. *Meteorit. & Planet. Sci*., **40**, 745–754.

Verma H.C., Rawat A., Paliwal B.S., Tripathi R.P. 2002. Mössbauer Spectroscopic Studies of an Oxidized Ordinary Chondrite Fallen at Itawa-Bhopji, India. *Hyperfine Interact*., **142**, 643–652.

Verma H.C., Jee K., Tripathi R.P. 2003. Systematics of Mössbauer absorption areas in ordinary chondrites and applications to newly fallen meteorite in Jodhpur, India. *Meteorit. & Planet. Sci*., **38**, 963–967.

Verma H.C., Tripathi R.P. 2004. Anomalous Mössbauer parameters in the second generation regolith Ghubara meteorite. *Meteorit. Planet. Sci*., **39**, 1755–1759.

Wang L., Moon N., Zhang Y., Dunham W.R., Essene E.J. 2005. Fe-Mg order-disorder in orthopyroxenes. *Geochim. Cosmochim. Acta*, **69**, 5777–5788.

Yudin I.A., Kozmanov Yu.D., Remennikova I.M. 1968. Investigation of minerals in the fusion crust of Saratov meteorite. *Meteoritics (Moscow)*, **28**, 156–157 (in Russian).

Zema M., Domeneghetti M.C., Tazzoli V. 1999. Order-disorder kinetics in orthopyroxene with exsolution products. *Am. Mineral*., **84**, 1895–1901.

Table 1. Averaged ranges of metals in selected minor iron-bearing phases in the polished thin section of Ozerki L6 ordinary chondrite obtained using energy dispersive spectroscopy.

Minor phases	wt.%
α-Fe(Ni, Co)	
Fe	92.2–95.3
Ni	2.8–6.0
Co	1.6–2.9
α₂-Fe(Ni, Co)	
Fe	74.6–86.2
Ni	12.0–23.8
Co	1.8–2.5
γ-Fe(Ni, Co)	
Fe	49.5–63.7
	69.4–71.4
Ni	27.2–28.2
	34.9–49.4
Co	0.5–2.4
γ-Fe(Ni, Co) par[a]	
Fe	66.0–69.4
Ni	29.0–33.1
Co	1.4–1.9
FeCr₂O₄	
Fe	9.3–9.8
Cr	15.6–17.4
Al	2.9–3.0
Ti	0.8–1.0
Mg	1.3–1.6
Mn	0.8–0.9

[a]"Par" means the paramagnetic state of the γ-phase.

Table 2. The unit cell parameters for silicate crystals in the bulk interior of Ozerki L6 ordinary chondrite obtained from X-ray diffraction.

Silicate crystals	Unit cell parameters			
	a, Å	*b*, Å	*c*, Å	β, °
Olivine	10.271(3)	6.012(3)	4.772(2)	–
Orthopyroxene	18.276(4)	8.867(3)	5.207(3)	–
Ca-rich clinopyroxene	9.75(5)	8.90(4)	5.28(4)	106.1

Table 3. Mössbauer parameters obtained for the Ozerki L6 bulk interior.

Γ, mm/s	δ, mm/s	$\Delta E_Q/2\varepsilon$, mm/s	H_{eff}, kOe	A, %	Component[a]
0.296±0.030	0.018±0.015	–0.060±0.015	341.5±0.5	5.10	α-Fe(Ni, Co)
0.296±0.030	0.014±0.015	–0.039±0.015	331.0±0.5	6.26	α-Fe(Ni, Co)
0.275±0.030	0.774±0.015	*ND*[b]	314.4±0.5	15.83	Troilite
0.234±0.030	1.186±0.015	3.005±0.015	–	29.35	Olivine M1
0.234±0.030	1.096±0.015	2.948±0.015	–	19.83	Olivine M2
0.234±0.030	1.129±0.015	2.331±0.015	–	4.53	Orthopyroxene M1
0.234±0.030	1.148±0.015	2.120±0.015	–	14.42	Orthopyroxene M2
0.234±0.030	0.900±0.018	1.347±0.037	–	0.66	Hercynite
0.689±0.060	0.598±0.022	–	–	2.35	Chromite
0.296[c]	0.102±0.015	–	–	1.68	Paramagnetic γ-Fe(Ni, Co)

[a]Components correspond to the spectral components shown in Fig. 5. [b]*ND* is non-determined. [c]Fixed parameter.

Table 4. The ratios of Fe^{2+} occupancies in the M1 and M2 sites in olivine and orthopyroxene microcrystals in the bulk interior of Ozerki L6 ordinary chondrite calculated using X-ray diffraction and Mössbauer spectroscopy data.

Silicate crystals	Method of estimation			
	XRD			Mössbauer spectroscopy
	X_{Fe}^{M1}	X_{Fe}^{M2}	X_{Fe}^{M1}/X_{Fe}^{M2}	A_{Fe}^{M1}/A_{Fe}^{M2}
Olivine	0.27	0.19	1.42	1.48
Orthopyroxene	0.11	0.34	0.32	0.31

Table 5. Mössbauer parameters obtained for the Ozerki L6 fusion crust.

Γ, mm/s	δ, mm/s	$\Delta E_Q/2\varepsilon$, mm/s	H_{eff}, kOe	A, %	Component[a]
0.329±0.030	0.277±0.015	–0.026±0.015	484.0±0.5	8.22	$MgFe_2O_4$ (A1)
0.317±0.043	0.271±0.015	–0.078±0.015	469.4±1.0	3.56	$MgFe_2O_4$ (A2)
0.747±0.055	0.721±0.016	–0.188±0.023	467.0±0.9	9.78	$MgFe_2O_4$ (B1)
0.318±0.067	0.538±0.020	0.373±0.036	447.7±1.6	1.51	$MgFe_2O_4$ (B2)
0.776±0.078	0.781±0.021	0.089±0.045	413.4±1.6	4.62	$MgFe_2O_4$ (B3)
0.348±0.030	0.041±0.015	0.003±0.015	337.2±0.5	6.08	α-Fe(Ni,Co)
0.269±0.030	0.773±0.015	*ND*[b]	312.2±0.5	4.62	Troilite
0.262±0.030	1.183±0.015	2.966±0.015	–	23.69	Olivine M1
0.262±0.030	1.104±0.015	2.887±0.015	–	19.35	Olivine M2
0.262±0.030	1.327±0.016	2.689±0.035	–	1.57	Orthopyroxene M1
0.262±0.030	1.150±0.015	2.091±0.015	–	7.36	Orthopyroxene M2
0.495±0.071	0.927±0.038	1.665±0.067	–	3.05	Ferrous compound
0.656±0.058	0.325±0.023	1.269±0.051	–	5.23	Ferric compound
0.778±0.401	0.748±0.065	–	–	1.37	Chromite

[a]Components correspond to the spectral components shown in Fig. 11. [b]*ND* is non-determined.

Table 6. The ratios of Fe^{2+} occupancies in the M1 and M2 sites in olivine and orthopyroxene microcrystals in the fusion crust of Ozerki L6 ordinary chondrite calculated using X-ray diffraction and Mössbauer spectroscopy data.

Silicate crystals	Method of estimation			
	XRD			Mössbauer spectroscopy
	X_{Fe}^{M1}	X_{Fe}^{M2}	X_{Fe}^{M1}/X_{Fe}^{M2}	A_{Fe}^{M1}/A_{Fe}^{M2}
Olivine	0.25	0.21	1.19	1.22
Orthopyroxene	0.08	0.36	0.22	0.21

Fig. 1.
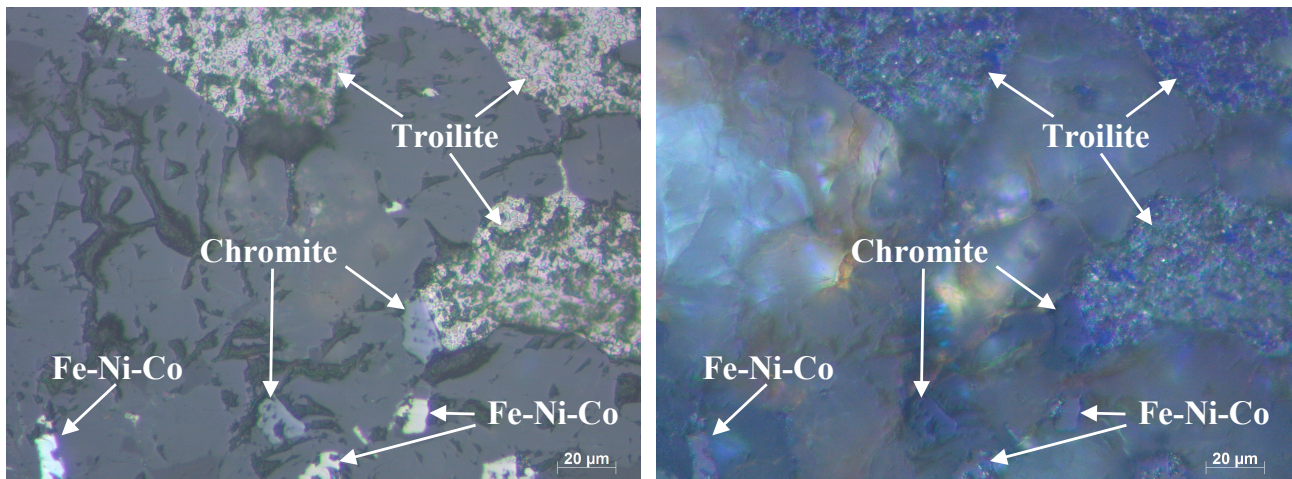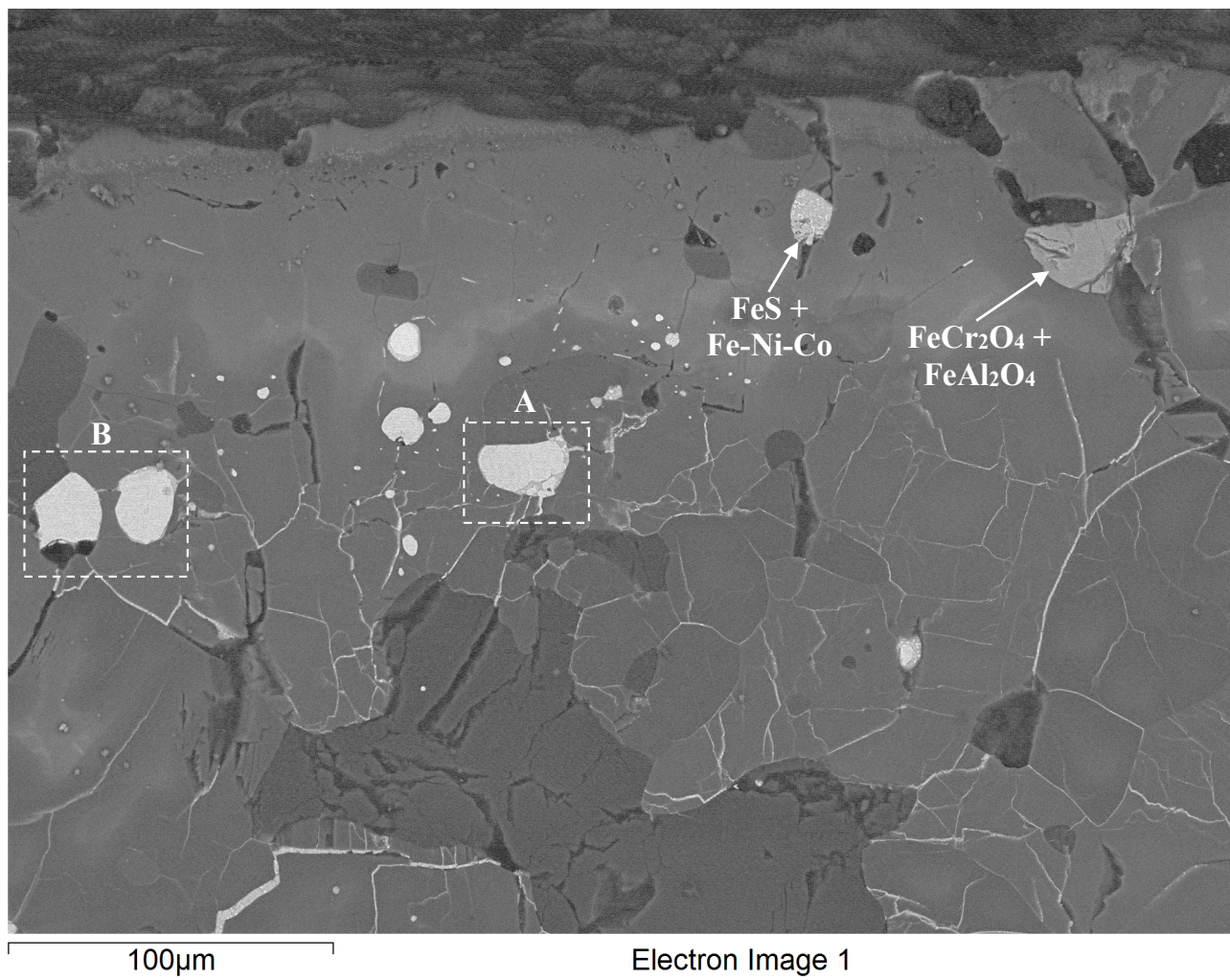
Fig. 2.
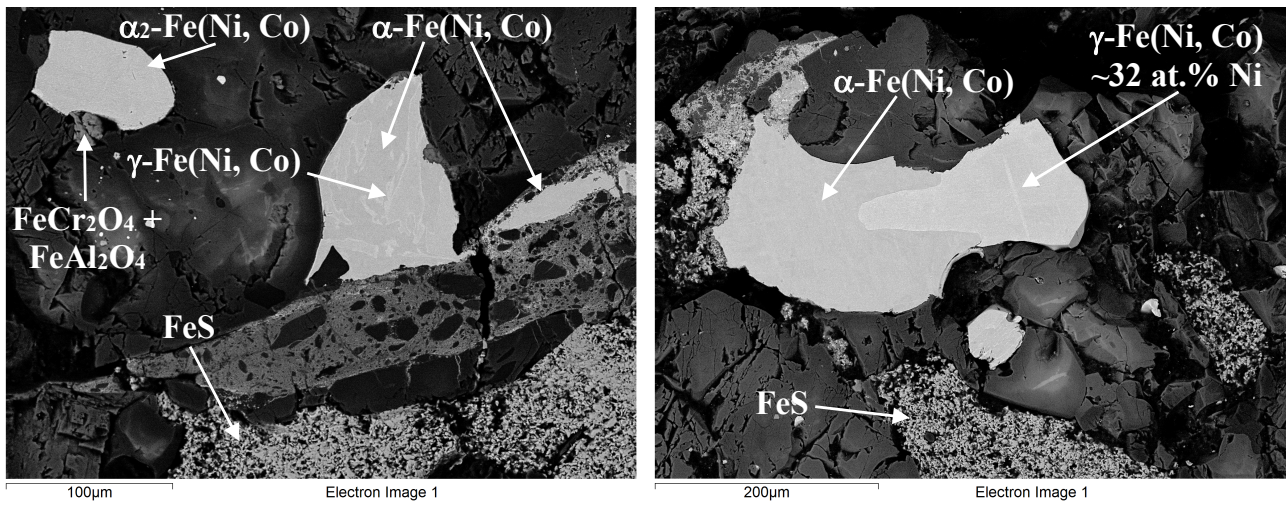
Fig. 3.
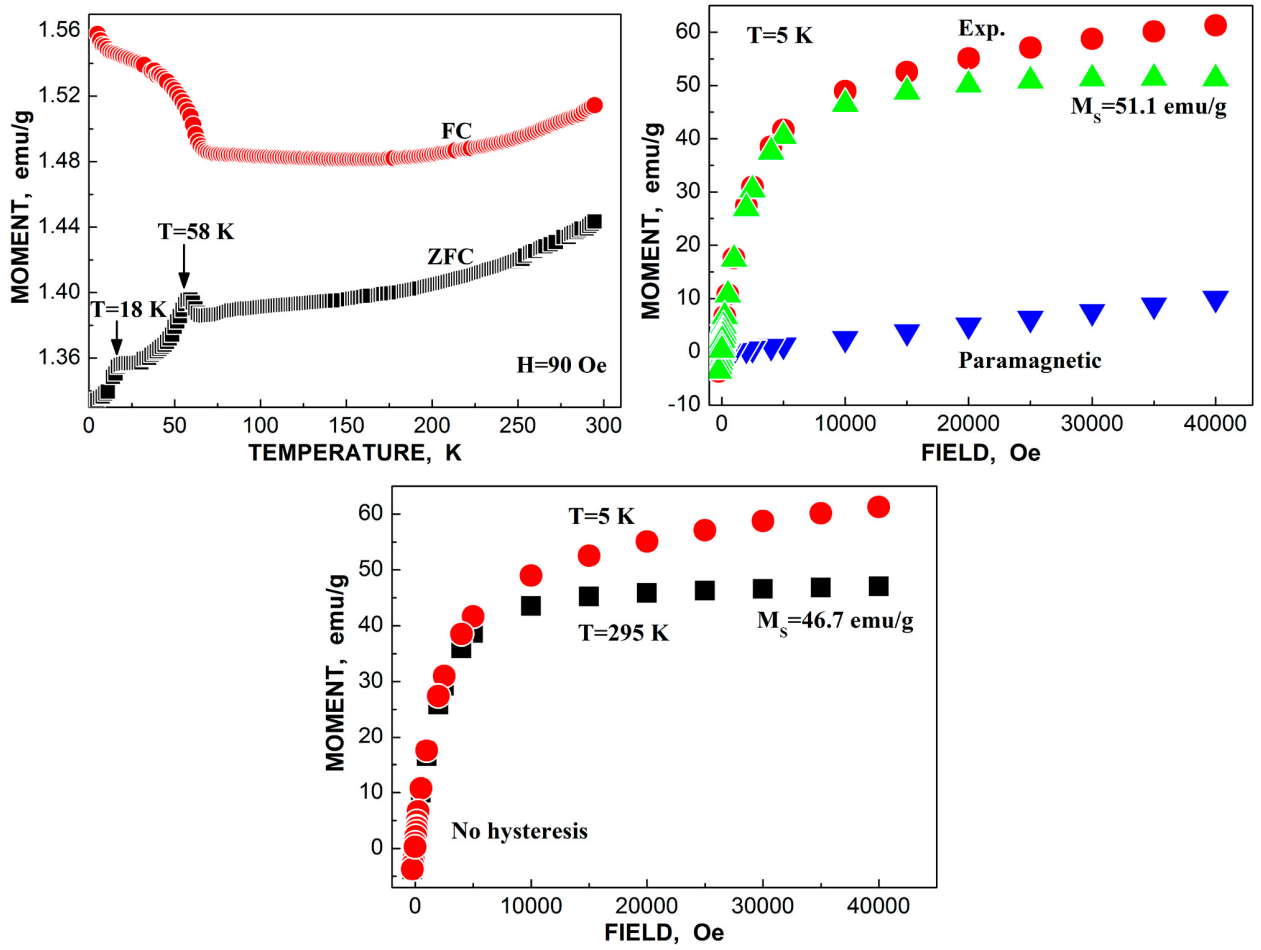
Fig. 4.
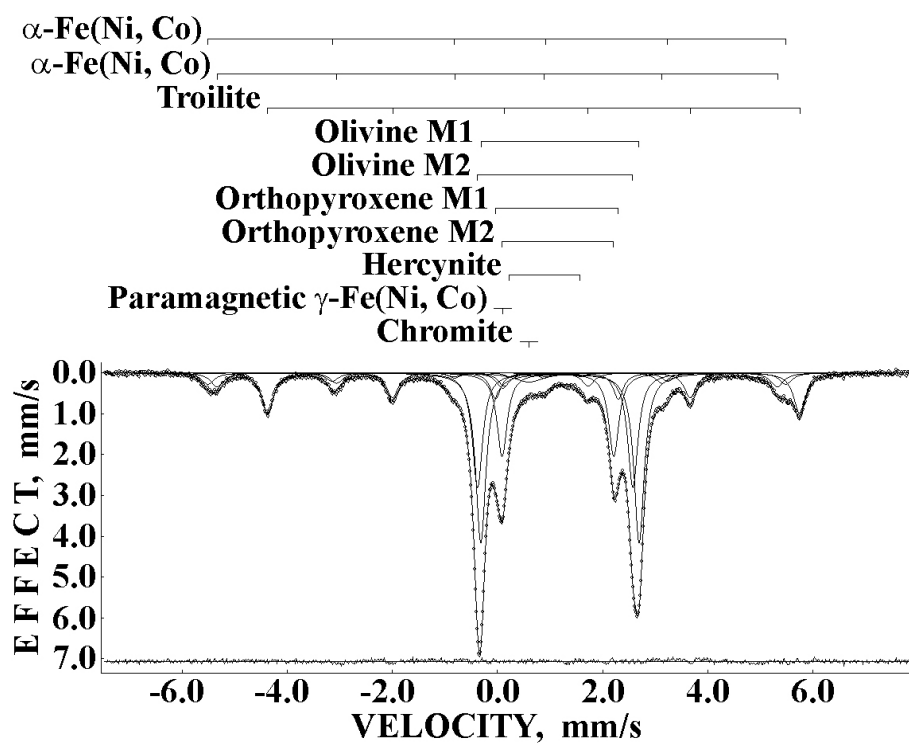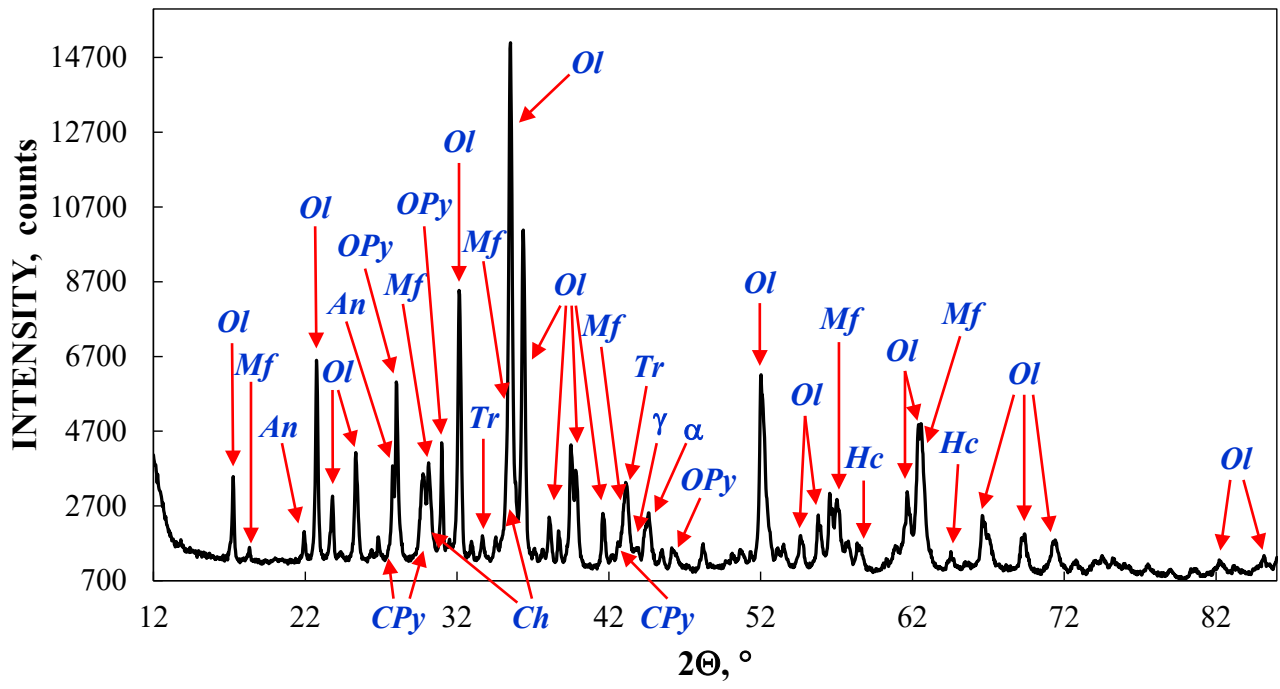
Fig. 5.
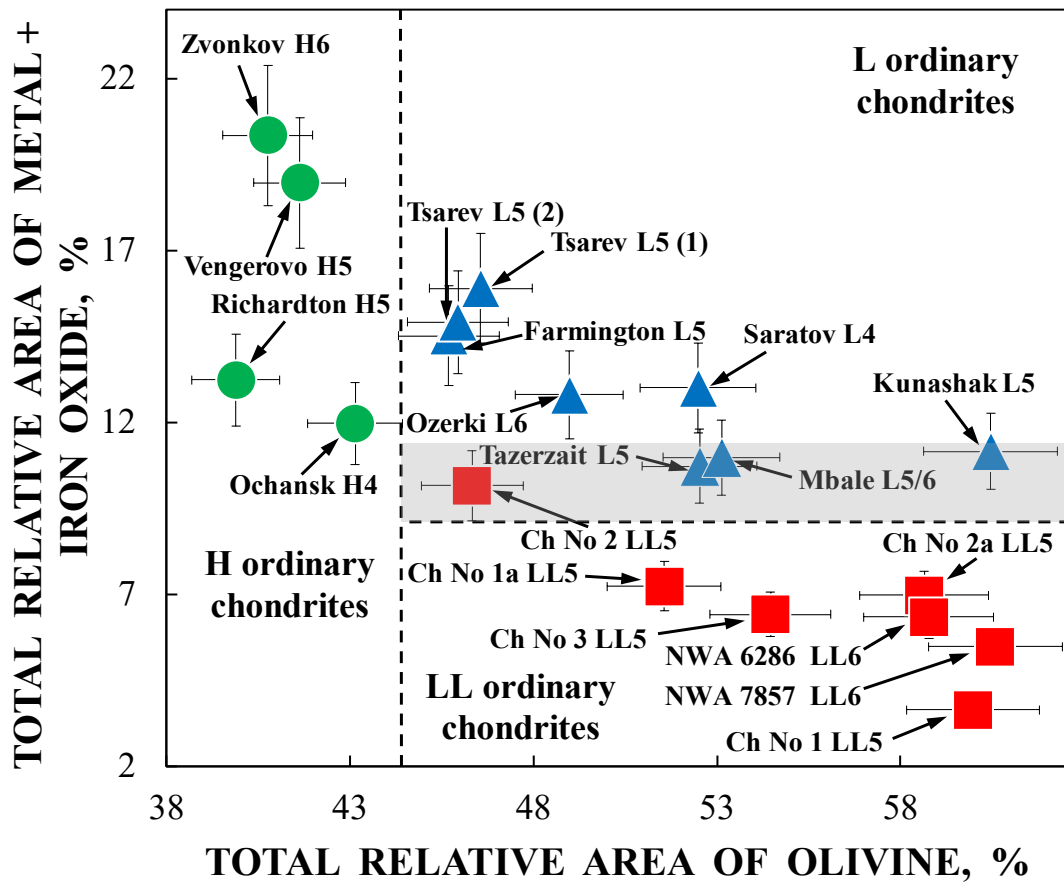
Fig. 6.
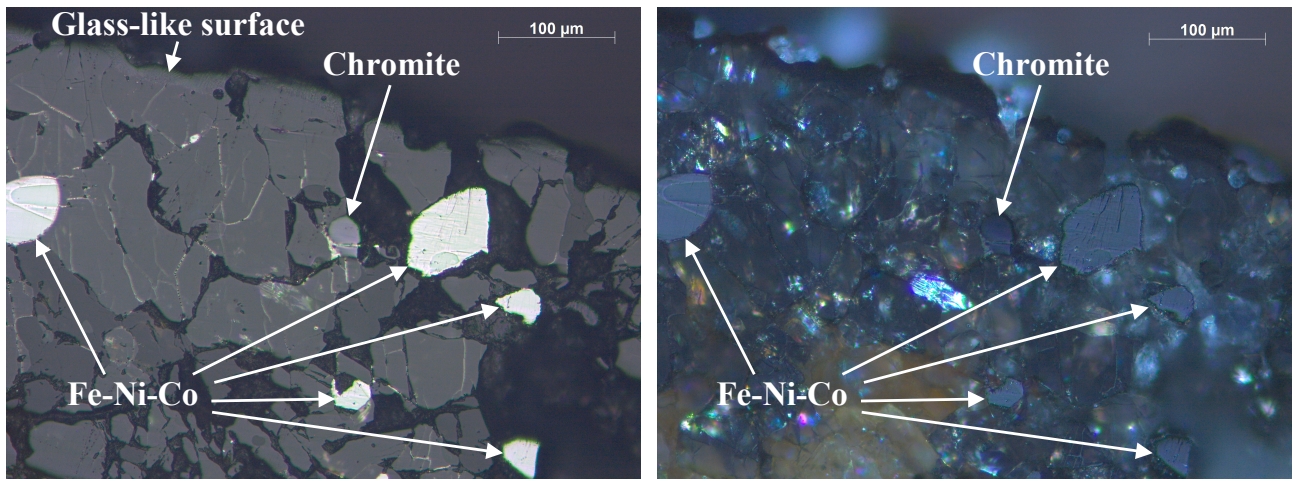
Fig. 7.

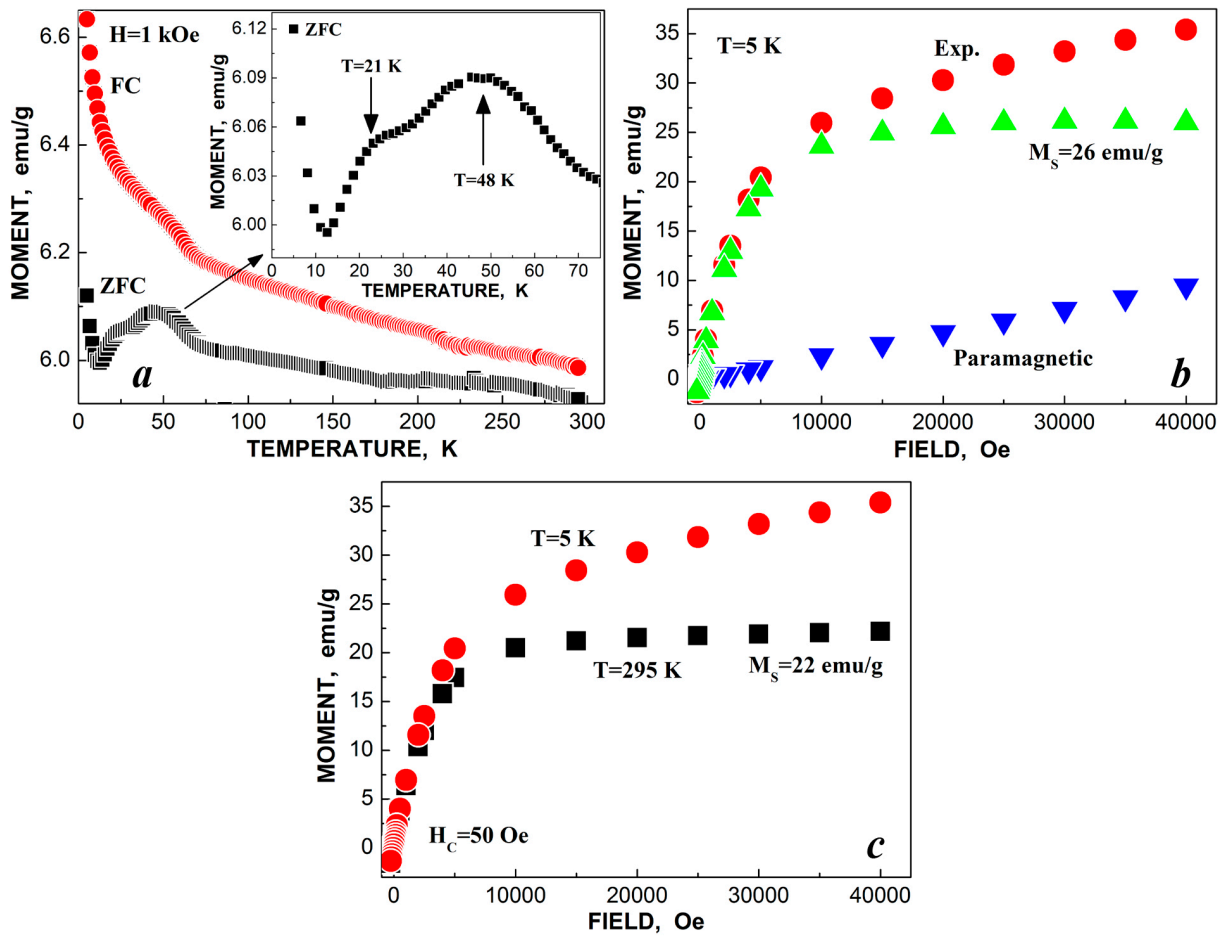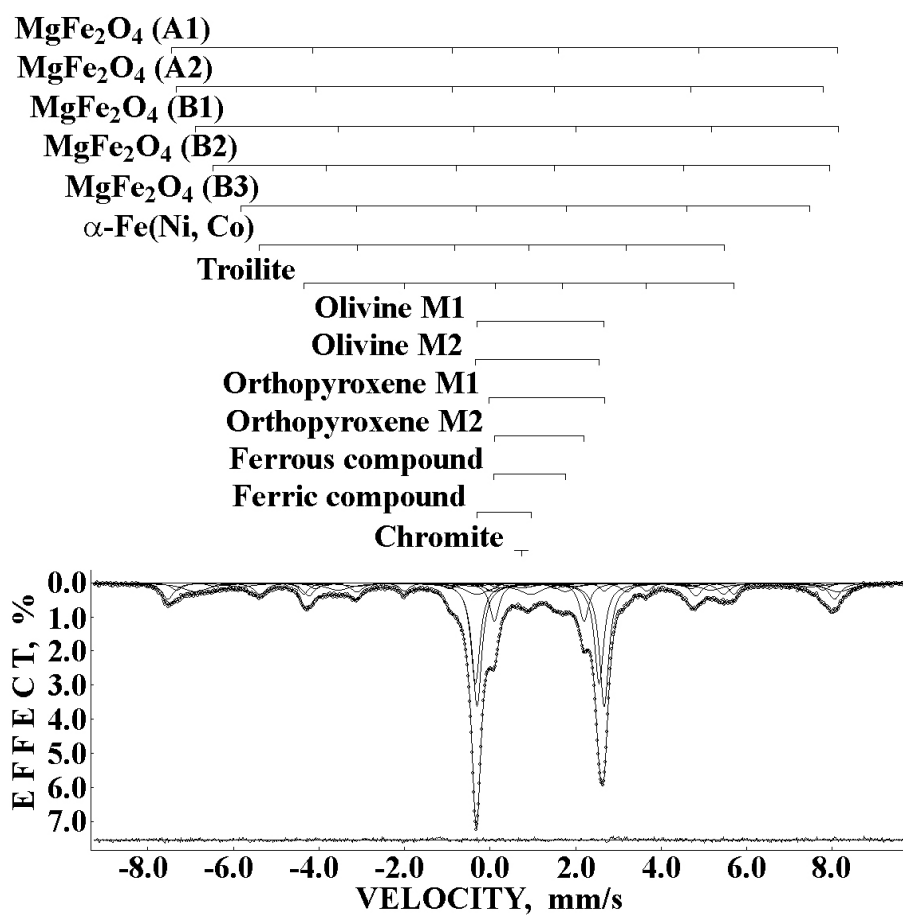Fig. 8.

Fig. 8.

Fig. 9.

Fig. 10.

Fig. 11.

FIGURE LEGENDS

Fig. 1. Photograph of the studied fragment of Ozerki L6 ordinary chondrite. The fusion crust can be seen on the top of this fragment.

Fig. 2. Selected microphotographs of the polished thin section of Ozerki L6 ordinary chondrite obtained in nonpolarized (left) and polarized (right) light.

Fig. 3. Selected scanning electron microscopy images of the polished thin section of Ozerki L6 ordinary chondrite. Indicated phases were determined using energy dispersive spectroscopy (see also Fig. S1 in Supporting Information).

Fig. 4. Zero-field cooled (ZFC) and field cooled (FC) magnetization curves and isothermal magnetization curves of the bulk interior of Ozerki L6 fragment. **Exp.** is experimental points, M_S is saturation magnetic moment, **T** is temperature.

Fig. 5. Mössbauer spectrum of the bulk interior of Ozerki L6 fragment. Indicated components are the results of the best fit. The differential spectrum is shown below. T=295 K.

Fig. 6. Systematics of H, L and LL ordinary chondrites using Mössbauer parameters with position for Ozerki L6 fragment. Abbreviations "Ch" and "NWA" mean "Chelyabinsk" and "Northwest Africa", respectively. Vertical and horizontal error bars are roughly estimated averaged relative errors. Adopted from Oshtrakh et al. (2019).

Fig. 7. Selected microphotographs of fusion crust at the polished thin section of Ozerki L6 ordinary chondrite obtained in nonpolarized (left) and polarized (right) light (the higher magnification images of the glass-like surface are shown in Fig. S3 in Supporting Information).

Fig. 8. Scanning electron microscopy image of the fusion crust at the polished thin section of Ozerki L6 ordinary chondrite. Indicated phases were determined using energy dispersive spectroscopy. Areas A and B are shown in Fig. S4 and the glass-like surface is shown in Fig. S5 with high magnifications in Supporting Information.

Fig. 9. X-ray diffraction pattern of the fusion crust from Ozerki L6 ordinary chondrite. ***Ol*** is olivine, ***An*** is anorthite, ***OPy*** is orthopyroxene, ***CPy*** is clinopyroxene, ***Tr*** is troilite, ***Ch*** is chromite, ***Hc*** is hercynite, ***Mf*** is magnesioferrite, α is α-Fe(Ni, Co) phase, γ is γ-Fe(Ni, Co) phase.

Fig. 10. Zero-field cooled (ZFC) and field cooled (FC) magnetization curves and isothermal magnetization curves of the fusion crust of Ozerki L6 fragment. **Exp.** is experimental points, M_S is saturation magnetic moment, **T** is temperature.

Fig. 11. Mössbauer spectrum of the fusion crust of Ozerki L6 fragment. Indicated components are the results of the best fit. The differential spectrum is shown below. T=295 K.